Inorganic Chemistry

ARTICLE

pubs.acs.org/IC

Syntheses, Crystal Structures, Magnetic and Luminescent Properties of two Classes of Molybdenum(VI) Rich Quaternary Lanthanide Selenites

Su-Yun Zhang[†,‡] and Jiang-Gao Mao*[,†]

[†]State Key Laboratory of Structural Chemistry, Fujian Institute of Research on the Structure of Matter, Chinese Academy of Sciences, Fuzhou 350002, P.R. China

[‡]Graduate School of the Chinese Academy of Sciences, Beijing 100039, P.R. China

Supporting Information

ABSTRACT: Hydrothermal reactions of lanthanide(III) oxide, molybdenum oxide, and SeO_2 at 230 °C lead to five new molybdenum-rich quaternary lanthanide selenites with two types of structures, namely, $H_3Ln_4Mo_{9.5}O_{32}(SeO_3)_4(H_2O)_2$ (Ln = La, **1**; Nd, **2**) and $Ln_2Mo_3O_{10}(SeO_3)_2(H_2O)$ (Ln = Eu, **3**; Dy, **4**; Er, **5**). Compounds **1** and **2** feature a complicated three-dimensional (3D) architecture constructed by the intergrowth of infinite molybdenum selenite chains of $[Mo_{4.75}SeO_{19}]^{5.5-}$ and one-dimensional (1D) lanthanide selenite chains. The structures of **3**, **4**, and **5** exhibit 3D network composed of 1D $[Mo_3SeO_{13}]^{4-}$ anionic chains connected by lanthanide selenite chains. The molybdenum selenite chain of $[Mo_{4.75}SeO_{19}]^{5.5-}$ in **1** and **2** is composed of a pair of $[Mo_3SeO_{13}]^{4-}$ chains as in **3**, **4**, and **5** interconnected by a $[Mo_{1.75}O_8]^{5.5-}$ double-strand polymer via corner-sharing. The lanthanide selenite chains in both structures are similar in terms of coordination modes of selenite groups as well as the coordination environments of lanthanide(III) ions. Luminescent studies at both room temperature and 10 K indicate that compound **2** displays strong luminescence in the near-IR region and compound **3** exhibits red fluorescent emission bands with a luminescent lifetime of 0.57 ms. Magnetic properties of these compounds have been also investigated.

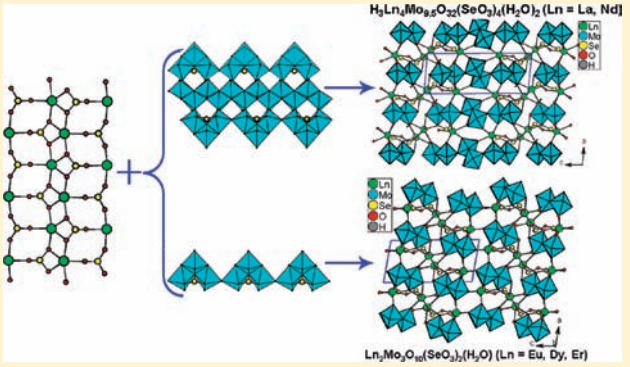

INTRODUCTION

Metal selenites and tellurites can form a diversity of unusual structures because of the presence of the stereochemically active lone-pair electrons which could serve as an invisible structure directing agent.[1] The asymmetric coordination polyhedron of the Se(IV) or Te(IV) atom caused by the so-called second-order Jahn−Teller (SOJT) distortion may also result in noncentrosymmetric (NCS) structures with consequent interesting physical properties, such as nonlinear optical second harmonic generation (SHG).[2] Transition metal ions with d^0 electronic configuration (such as Ti^{4+}, V^{5+}, W^{6+}, Mo^{6+}, etc.) which are susceptible to second-order Jahn−Teller distortions have been introduced to the selenite or tellurite systems to obtain compounds with good SHG properties considering the additive polarization of both types of bonds.[3−5] Most of these research efforts have been focused on alkali, alkaline earth, and NH_4^+ compounds which show potential application in SHG materials because of their broad transparency range and high transmittance in the ultraviolet and visible region.[4,5] Recently, similar phases of transition metal as well as the post transition metal main group cations have also been prepared.[6,7]

As for the corresponding lanthanide compounds, a number of ternary lanthanide selenites and tellurites have been reported.[1,8,9] A series of lanthanide selenites and tellurites with MO_6 or MO_4 (M = Mo, W) polyhedra have been synthesized by high-temperature solid state reactions, including $Nd_2MoSe_2O_{10}$, $Gd_2MoSe_3O_{12}$, $La_2MoTe_3O_{12}$, $Nd_2MoTe_3O_{12}$, $Ln_2(MoO_4)(Te_4O_{10})$ (Ln = Pr, Nd), $La_2(WO_4)(Te_3O_7)_2$, $Nd_2W_2Te_2O_{13}$, and $Ln_5(MO_4)(Te_5O_{13})(TeO_3)_2Cl_3$ (Ln = Pr, Nd; M = Mo, W).[10] Furthermore, several lanthanide selenites decorated by V^{5+} ions, namely, $Nd_2(V_2O_4)(SeO_3)_4(H_2O)$ and $Ln(VO_2)(SeO_3)_2$ (Ln = Eu, Gd, Tb), have been synthesized by hydrothermal reactions using V_2O_3 as vanadium resource.[11] They display a variety of interesting open-framework structures and some of them exhibit good luminescent properties.

It is also noticed that most of MoO_x (x = 4 or 6) polyhedra in the above compounds are not polymerized because of small Mo/Ln (≤1) ratios. $Nd_2MoSe_2O_{10}$ and $Gd_2MoSe_3O_{12}$ contain isolated MoO_4 tetrahedra and MoO_6 octahedra, respectively, whereas only isolated MoO_4 tetrahedra were found in the corresponding lanthanide tellurites. We deem that the MoO_4 or MoO_6 may polymerize into novel polynuclear clusters or

Received: January 22, 2011
Published: April 28, 2011

Table 1. Crystal Data and Structure Refinements for the Title Compounds

formula	$H_3La_4Mo_{9.5}O_{32}(SeO_3)_4(H_2O)_2$	$H_3Nd_4Mo_{9.5}O_{32}(SeO_3)_4(H_2O)_2$	$Eu_2Mo_3O_{10}(SeO_3)_2(H_2O)$	$Dy_2Mo_3O_{10}(SeO_3)_2(H_2O)$	$Er_2Mo_3O_{10}(SeO_3)_2(H_2O)$
Fw	2525.97	2543.25	1023.68	1044.76	1054.28
space group	$P\bar{1}$	$P\bar{1}$	$P2_1/m$	$P2_1/m$	$P2_1/m$
a/ Å	6.980(2)	6.878(6)	6.8535(14)	6.7806(9)	6.7465(14)
b/ Å	7.349(3)	7.289(7)	7.2488(11)	7.1875(6)	7.1715(14)
c/ Å	18.123(6)	17.875(2)	14.206(4)	14.1304(17)	14.082(4)
α/ deg	95.908(7)	95.786(16)	90	90	90
β/ deg	95.323(6)	95.203(9)	100.473(16)	100.318(7)	100.246(14)
γ/ deg	90.022(9)	90.176(2)	90	90	90
V/ Å^3	920.6(5)	887.8(1)	694.0(2)	677.52(13)	670.5(3)
Z	1	1	2	2	2
D_{calcd}/g cm^{-3}	4.556	4.755	4.899	5.121	5.222
μ(Mo-Kα)/mm^{-1}	11.736	12.74	16.880	19.062	20.634
GOF on F^2	1.011		1.050	0.991	1.199
R1, wR2 [$I > 2\sigma(I)$][a]	0.0313, 0.0675		0.0400, 0.0821	0.0240, 0.0551	0.0654, 0.1315
R1, wR2(all data)	0.0406, 0.0699		0.0460, 0.0857	0.0280, 0.0565	0.0827, 0.1437

[a] $R1 = \Sigma||F_o| - |F_c||/\Sigma|F_o|$, $wR2 = \{\Sigma w(F_o^2 - F_c^2)^2/\Sigma w(F_o^2)^2\}^{1/2}$.

extended structures through corner- or edge-sharing if the Mo/Ln ratios are larger (>1). Our explorations of Mo-rich Ln^{III}-Mo^{VI}–Se^{VI}-O phases led to five new lanthanide selenites containing MoO_6 octahedra, namely, $H_3Ln_4Mo_{9.5}O_{32}(SeO_3)_4(H_2O)_2$ (Ln = La, **1**; Nd, **2**) and $Ln_2Mo_3O_{10}(SeO_3)_2(H_2O)$ (Ln = Eu, **3**; Dy, **4**; Er, **5**). The MoO_6 octahedra in the above two classes of compounds are interconnected into two types of novel molybdenum oxide chains. Herein we report their syntheses, crystal structures, and luminescent and magnetic properties.

EXPERIMENTAL SECTION

Materials and Methods. All of the chemicals were analytically pure, obtained from commercial sources, and used without further purification. Molybdenum oxide or lanthanide oxides were purchased from the Shanghai Reagent Factory and SeO_2 (99+ %) was purchased from ACROS ORGANICS. Microprobe elemental analyses were performed on a field emission scanning electron microscope (FESEM, JSM6700F) equipped with an energy dispersive X-ray spectroscope (EDS, Oxford INCA). The X-ray powder diffraction data were collected on a XPERT-MPD θ-2θ diffractometer. Thermogravimetry analysis (TGA) studies were all carried out with a NETZSCH STA 449C instrument. The samples and reference (Al_2O_3) were enclosed in a platinum crucible and heated at a rate of 15 °C/min from room temperature to 1000 °C under a nitrogen atmosphere. The IR spectra were recorded on a Magna 750 FT-IR spectrometer as KBr pellets in the range of 4000−400 cm^{-1}. Elemental analyses on H element in compounds **1** and **2** were performed on a German Elementary Vario EL III instrument. Room temperature and low temperature luminescent properties were performed on an Edinburgh FLS920 fluorescence spectrometer. Magnetic susceptibility measurements on polycrystalline samples were performed with a PPMS-9T magnetometer at a field of 1000 Oe in the temperature range 2−300 K.[12]

Preparations of Compounds 1−5. The five compounds were initially synthesized by the hydrothermal reactions of a mixture of lanthanide oxide (0.1 mmol), molybdenum oxide (0.5 mmol), and selenium dioxide (1.0 mmol) in 5 mL of distilled water, which was sealed in an autoclave equipped with Teflon lining (25 mL) and heated at 230 °C for 4 days, followed by cooling at a rate of 5 °C/h to room temperature. The pH values of the reaction media before and after the reaction are close to 1.5 and 1.0 for all these compounds, respectively. Energy-dispersive spectrometry (EDS) elemental analyses give the molar ratios of La/Mo/Se of 1.0:2.7:1.0 for **1**, Nd/Mo/Se of 1.1:2.4:1.0 for **2**, Eu/Mo/Se of 1.0:1.7:1.1 for **3**, Dy/Mo/Se of 1.0:1.8:1.0 for **4** and Er/Mo/Se of 1.0:1.7:1.0 for **5**, which are in good agreement with those determined from single crystal X-ray structural analyses. The two types of compounds isolated under similar reactions are most probably due to "the lanthanide contraction". After proper structural analyses, compounds **1**−**5** were obtained as single phases by the hydrothermal reactions of a mixture of 0.1 mmol Ln_2O_3, 0.5 (for **1**−**2**) or 0.3 (for **3**−**5**) mmol MoO_3, 1.0 mmol SeO_2 and H_2O (5 mL) at 230 °C for 4 days. The yields are about 40%, 46%, 38%, 35%, and 31% (based on Mo), respectively for **1**−**5**. Their purities were confirmed by X-ray powder diffraction studies (Supporting Information, Figure S1).

X-ray Crystallography. Single crystals of compounds **1** and **3**−**5** were analyzed on either a Rigaku Mercury CCD diffractometer (for **3** and **5**) or SATURN 70 CCD diffractometer (for **1** and **4**) equipped with a graphite-monochromated Mo-Kα radiation (λ = 0.71073 Å) at 293 K. The data sets were corrected for Lorentz and polarization factors as well as for absorption by the Multiscan method.[13a] All structures were solved by direct methods and refined by full-matrix least-squares fitting on F^2 by SHELX-97.[13b] The structure was checked with PLATON.[13c] All non-hydrogen atoms were refined with anisotropic thermal parameters except O(2) atom in compound **1**, which was refined isotropically because of its large ADP max/min ratio. The Mo(4) site in compound **1** was initially refined with full occupancy, which resulted in a very large atomic displacement parameter of 0.02176 Å^2 in comparison with those of other four Mo atoms (0.00362, 0.00311, 0.00329, and 0.00368 Å^2), with relatively high R1 of 0.0430 and wR2 of 0.0559. Subsequently, the occupancy of Mo(4) was allowed to be refined, which converged to close to 75%, with a comparable displacement factor of 0.00462 Å^2 and lower R values of R1 = 0.0313 and wR2 = 0.0406. The partial occupancy of the Mo(4) site led to the excessive negative charges which needed additional 1.5 protons for charge balance. The H content determined by element analysis is 0.24% (the calculated value is 0.28% containing the additional protons), which provided further evidence of the existence of the protons. Similar cases have been observed in other polymolybdates and polytungstates.[14] However, these protons were not refined because of the difficulty in determining their exact locations. Hence, the final formula was refined to be $H_3La_4Mo_{9.5}O_{32}(SeO_3)_4(H_2O)_2$. A relatively high residual of 3.70 e Å^{-3} is found in $H_3La_4Mo_{9.5}O_{32}(SeO_3)_4(H_2O)_2$, which is 1.09 Å from the Se(2) atoms; hence, it can be regarded as a ghost peak. Hydrogen

dx.doi.org/10.1021/ic200149y |Inorg. Chem. 2011, 50, 4934–4943

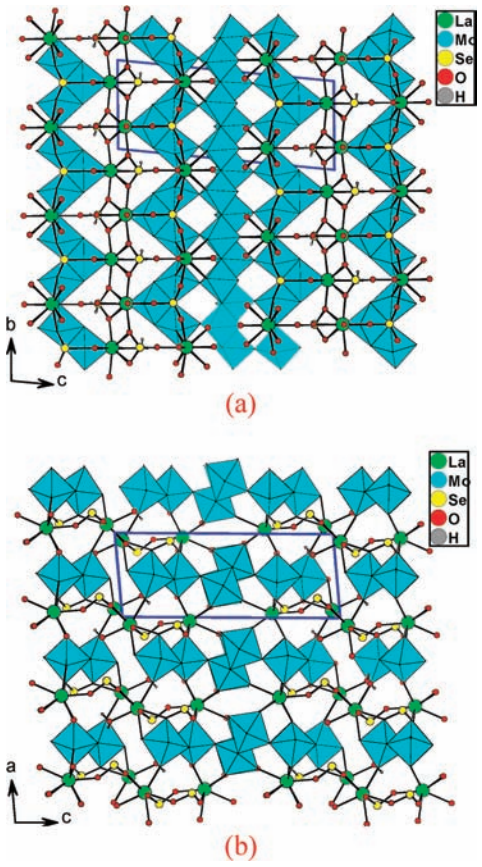

Figure 1. View of the 3D structure of compound **1** down the *a*-axis (a) and *b*-axis (b). MoO_6 octahedra are shaded in cyan. La, Se, and O atoms are represented by green, yellow, and red circles, respectively.

atoms associated with the aqua ligands in these compounds were located at geometrically calculated positions and refined with isotropic thermal parameters. Compound **2** is isostructural with Compound **1** based on its cell parameters (triclinic with $a = 6.878(6)$, $b = 7.289(7)$, $c = 17.875(17)$ Å, $\alpha = 95.786(16)$, $\beta = 95.203(9)$, $\gamma = 90.176(16)$ °, $V = 887.8(14)$ Å^3) and powder X-ray diffraction. Its data collection was not performed because of bad quality of its single crystals. Crystallographic data and structural refinements for compounds **1**, **3**, **4**, **5** and cell parameters for compound **2** are summarized in Table 1. Important bond distances are listed in Supporting Information, Table S1.

RESULT AND DISCUSSION

Hydrothermal reactions of lanthanide oxide, MoO_3 and SeO_2 lead to five new Mo-rich lanthanide molybdenum selenites with two different types of structures, namely, $H_3Ln_4Mo_{9.5}O_{32}(SeO_3)_4(H_2O)_2$ (Ln = La, **1**; Nd, **2**) and $Ln_2Mo_3O_{10}(SeO_3)_2(H_2O)$ (Ln = Eu, **3**; Dy, **4**; Er, **5**). Their structures are totally different from the lanthanide molybdenum selenites and tellurites prepared by high-temperature solid state reactions previously reported.[10] The Mo/Ln ratios in the above compounds are 5/2 and 3/2, respectively. The MoO_6 octahedra had polymerized into infinite chains under strong acidic environment. The reported phases in Ln^{III}-Mo^{VI}-Se^{IV}/Te^{IV}-O systems prepared by solid state reactions at 750 or 700 °C have a Mo/Ln ratio of 1/2 or 1/5,[10] the Ln^{3+} ions are bridged by SeO_3^{2-} or various tellurite anions into three-dimensional (3D) architectures or two-dimensional (2D) layers whereas the "isolated" MoO_6 or MoO_4 occupied the apertures in the 3D networks as in $Gd_2Mo_3Se_3O_{12}$ and $La_2MoO_4(Te_3O_8)$, or hanging on the lanthanide selenite or tellurite layer as in $Nd_2(MoO_4)(TeO_3)(Te_2O_5)$ or acting as the pillars between two neighboring layers as in $Ln_2(MoO_4)(Te_4O_{10})$ (Ln = Pr, Nd).[10] Hence, the large Mo/Ln ratios as well as the strong acidic reaction media play an important role in the polymerization of the MoO_6 octahedra in the five compounds.

Structural Descriptions. $H_3Ln_4Mo_{9.5}O_{32}(SeO_3)_4(H_2O)_2$ (Ln = La, **1**; Nd, **2**) features a complicated 3D network in which the molybdenum selenite chains are further interconnected by lanthanide selenite chains (Figure 1). The structure of compound **1** will be discussed in detail as a representative compound. There are two La(III) atoms, five Mo(VI) atoms, and two Se(IV) atoms in the asymmetric unit. La(1) is eight-coordinated by one aqua ligand, five selenite oxygens and two oxygens from molybdate anions whereas La(2) is nine-coordinated by three selenite oxygens and six oxygens from molybdate anions. The La−O distances range from 2.429(6) to 2.621(6) Å (Supporting Information, Table S1), which are comparable to those in other lanthanide(III) selenites reported.[10,15] All the five unique Mo atoms are octahedrally coordinated. Mo(1), Mo(2), and Mo(3) are surrounded by five bridging oxo anions and one selenite oxygen. Mo(4) is octahedrally coordinated by five bridging oxo anions and one terminal O^{2-} anion whereas Mo(5) is coordinated by six bridging oxo anions. All five Mo(VI) atoms are in severely distorted octahedral coordination environments exhibiting similar bond and angle characteristics with two "short" (1.695(8)−1.742(6) Å), two "normal" (1.891(6)−1.964(6) Å) and two "long" (2.126(6)−2.401(6) Å) Mo−O bonds. The O−Mo−O bonds angles also deviate greatly from the ideal 90° and 180°, being in the range of 71.0(2)−107.9(3) ° for cis O−Mo−O bonds and 140.9(2)−176.1(2) ° for trans ones. Such MoO_6 octahedra are distorted toward an edge (local C_2 direction). Taking into account the six Mo−O bond lengths as well as the deviation from 180° of the three trans O−Mo−O bond angles of each MoO_6 octahedra, the magnitudes of the distortion (Δd) were calculated to be 1.155, 1.025, 0.985, 1.371, 1.199 Å, respectively.[16] It is also noticed that the MoO_6 polyhedra are distorted away from the oxygen atoms bonded to Se^{4+} cations as in other metal selenites with distorted MoO_6 octahedra,[17] which is due to the distortion of the lone-pair electrons as well as the structural rigidity of the SeO_3^{2-} groups. The Se(IV) cations are coordinated by three oxygen atoms in a distorted ψ-SeO_3 trigonal-pyramidal geometry with the lone pair of Se(IV) occupying the pyramidal site. The Se−O distances fall in the normal range of 1.692(6)−1.731(5) Å (Supporting Information, Table S1). Bond valence calculations indicate that La, Mo, and Se atoms are in oxidation states of +3, +6, and +4, respectively. The calculated total bond valences for two La, five Mo, and two Se atoms are 3.28, 3.12, 5.89, 6.02, 6.04, 5.72, 6.00, 3.93, and 3.86, respectively.[18]

The interconnection of $La(1)^{3+}$ and $La(2)^{3+}$ ions by bridging SeO_3^{2-} groups resulted in a lanthanide selenite chain along the *b*-axis (Figure 2a). The intrachain La···La distances are in the range of 4.120(1) and 7.349(1) Å.

The $Mo(1)O_6$, $Mo(2)O_6$, $Mo(3)O_6$ octahedra are interconnected by edge-sharing bonds (O(7)···O(10) and O(11)···O(10)) forming a $[Mo_3O_{14}]^{10-}$ trimer, and O(10) is a μ_3 metal linker and bridges with Mo(1), Mo(2), and Mo(3) atoms. The $Se(2)O_3^{2-}$ group is capped on the trimer via Se−O−Mo bridges, forming a $[Mo_3SeO_{14}]^{6-}$ unit. Such units are further connected into a molybdenum selenite chain $[Mo_3SeO_{13}]^{4-}$ via corner-sharing

dx.doi.org/10.1021/ic200149y |*Inorg. Chem.* 2011, 50, 4934–4943

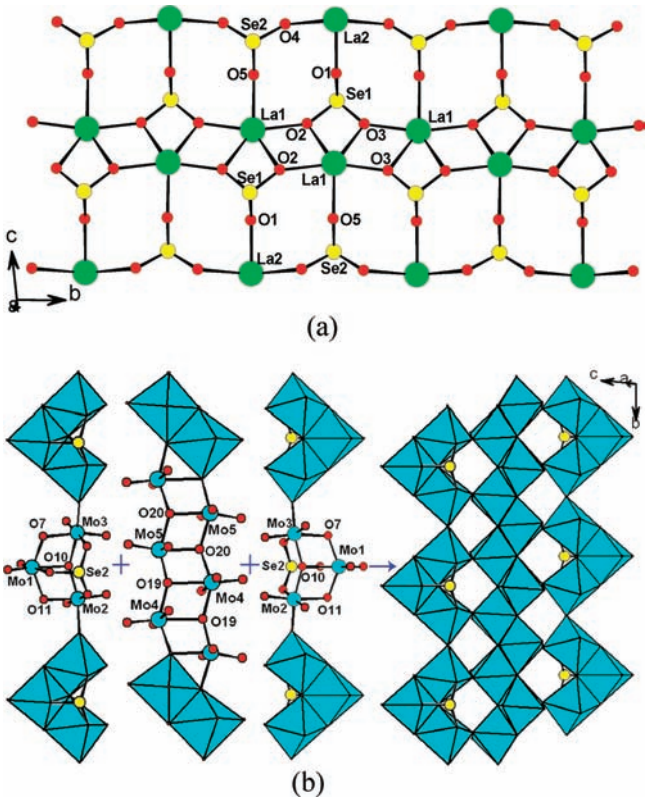

Figure 2. 1D lanthanide selenite chain along the *b*-axis in compound **1** (a), the $[Mo_{1.75}O_8]^{-5.5}$ chain and the $[Mo_3SeO_{13}]^{4-}$ chain and a molybdenum selenite ribbon of $[Mo_{4.75}SeO_{19}]^{5.5-}$ formed by the two chains (b). MoO_6 octahedra are shaded in cyan. La, Se, and O atoms are represented by green, yellow, and red circles, respectively.

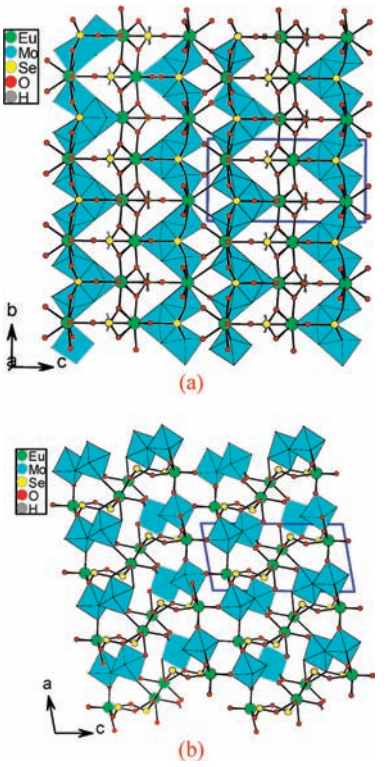

Figure 3. View of the 3D structure of compound **3** down the *a*-axis (a) and *b*-axis (b). MoO_6 octahedra are shaded in cyan. Eu, Se, and O atoms are represented by green, yellow, and red circles, respectively.

(O(16)) along the *b*-axis. The Mo···Mo distances in the trimer are 3.289(1) and 3.771(1) Å and that of the intercluster one is 3.578(1) Å. A pair of $Mo(4)O_6$ octahedra are connected into a $[Mo_{1.5}O_{11}]^{13-}$ dimer through the O(19)···O(19) edge, and so a pair of $Mo(5)O_6$ octahedra through the O(20)···O(20) edge. The interconnection of $[Mo(4)_{1.5}O_{11}]^{13-}$ and $[Mo(5)_2O_{11}]^{10-}$ through sharing the O(19)···O(20) edge resulted in a double-strand polymer $[Mo_{1.75}O_8]^{5.5-}$ with the Mo···Mo distance in the range of 3.291(1) and 3.373(1) Å. Both O(19) and O(20) act as μ_3 metal linkers each bridging with three Mo atoms. A pair of $[Mo_3SeO_{13}]^{4-}$ chains are sandwiched by the $[Mo_{1.75}O_8]^{5.5-}$ chain through Mo(3)−O(16)−Mo(4) and Mo(2)−O-(12)−Mo(5) bridges into a thick slab of $[Mo_{4.75}SeO_{19}]^{5.5-}$ with interchain Mo···Mo distances of 3.856(1) and 3.897(1) Å (Figure 2b).

The lanthanide selenite chains and the molybdenum selenite ribbons are parallel to each other and are alternatively arranged along the *a*-axis (Figure 1a). The above two types of chains are further interconnected into a 3D network via La−O−Mo bridges (Figure 1b). The $Se(1)O_3$ group serves as a tetradentate metal linker and bonds to three La(1) and one La(2) atoms whereas the $Se(2)O_3$ group serves as a hexadentate metal linker and bonds to three La(III) atoms (one La(1), two La(2)) and three Mo(VI) atoms (one Mo(1), one Mo(2), and one Mo(3)).

$Ln_2Mo_3O_{10}(SeO_3)_2(H_2O)$ (Ln = Eu, **3**; Dy, **4**; Er, **5**) with lower Ln/Mo molar ratio was obtained for the heavier lanthanide elements. Their structures feature a 3D framework also constructed by the intergrowth of the molybdenum selenite chains and the lanthanide selenites chains (Figure 3). Since these three compounds are isostructural to each other only the structure of compound **3** will be discussed in detail as representative. The asymmetric unit of **3** contains two Eu^{3+} (both located on the mirror planes), two Mo^{6+} (one at general position and the other located on the mirror plane), two Se^{4+} (both located on the mirror planes) ions, and an aqua ligand. Eu(1) is eight-coordinated by five selenite oxygens, two oxo anions, and one aqua ligand whereas Eu(2) is coordinated by three selenite oxygens and five oxo anions. The Eu−O distances range from 2.264(9) to 2.495(5) Å (Supporting Information, Table S1). The Mo(1) and Mo(2) are in distorted octahedral geometry, being coordinated by five bridging oxo anions and one selenite anion. The Mo−O distances range from 1.715(9) to 2.358(7) Å, with two "short" (1.716(5)−1.739(9) Å), two "long" (2.066(6)−2.359(7) Å) and two "normal" (1.893(5)−1.962(3) Å) Mo−O bonds (Supporting Information, Table S1). The O−Mo−O bonds angles fall in the range of 137.2(4)−179.7(4) ° for the trans ones, 71.5 (2)−105.0(4) ° for the cis ones. So $Mo(1)O_6$ and $Mo(2)O_6$ are distorted toward an edge (local C_2 direction). Taking into account the six Mo−O bond lengths as well as the deviation from 180° of the three trans O−Mo−O bond angles of each MoO_6 octahedra, the magnitudes of the distortion (Δd) were calculated to be 0.966 and 1.122 Å,[16] respectively for $Mo(1)O_6$ and $Mo(2)O_6$, which are comparable to those in compound **1**. The Se(IV) cations are coordinated by three oxygen atoms in a distorted ψ-SeO_3 trigonal-pyramidal geometry with the lone pair of Se(IV) occupying the pyramidal site. The Se−O distances fall in the normal range of 1.691(9)−1.714(5) Å (Supporting Information, Table S1). Bond valence calculations indicate that Eu, Mo, and Se atoms are in oxidation states of +3, +6, and +4,

dx.doi.org/10.1021/ic200149y |*Inorg. Chem.* 2011, 50, 4934–4943

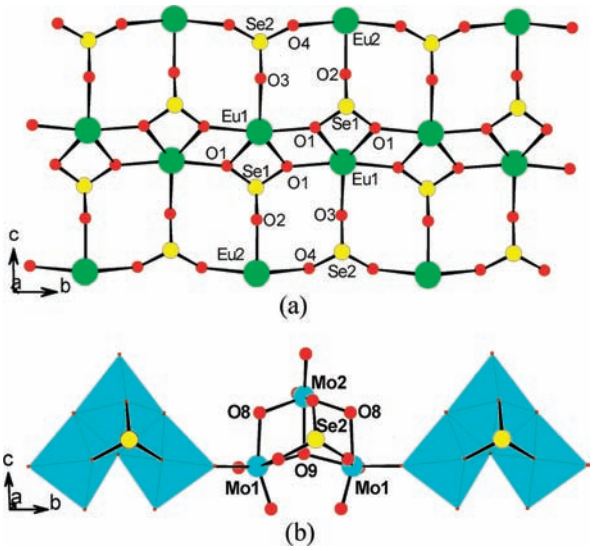

Figure 4. 1D europium selenite chain along the *b*-axis in compound **3** (a) and a $[Mo_3SeO_{13}]^{4-}$ chain along the *b*-axis (b). MoO_6 octahedra are shaded in cyan. Eu, Se, and O atoms are represented by green, yellow, and red circles, respectively.

respectively. The calculated total bond valences for Eu(1), Eu(2), Mo(1), Mo(2), Se(1), and Se(2) atoms are 2.82, 3.22, 6.07, 6.08, 3.98, and 3.94, respectively.[18]

The interconnection of $Eu(1)^{3+}$ and $Eu(2)^{3+}$ ions through bridging $Se(1)O_3^{2-}$ and $Se(2)O_3^{2-}$ groups led to a europium selenite chain along the *b*-axis (Figure 4a). The Eu···Eu distances within the chain are in the range of 4.052(7) and 7.249(1) Å. It should be mentioned that the europium selenite chain is identical with the lanthanide selenite chain in compound **1**.

Two $Mo(1)O_6$ and one $Mo(2)O_6$ octahedra are interconnected by edge-sharing (O(8)···O(9)) into a $[Mo_3O_{14}]^{10-}$ trimer. O(9) is a μ_3 metal linker, bridging with two Mo(1) and one Mo(2) atoms. The $[Mo_3O_{14}]^{10-}$ trimer is further capped by Se(2) atoms into a $[Mo_3SeO_{14}]^{6-}$ unit. Neighboring $[Mo_3SeO_{14}]^{6-}$ units are further interconnected via corner-sharing into a molybdenum selenite chain as in compound **1** (Figure 4b). The Mo···Mo distances within the trimer are 3.256(1) and 3.690(1) Å whereas the shortest intercluster one is 3.559(1) Å.

The interconnection of the alternating europium selenite and molybdenum selenite chains along the *a*-axis via Mo-O-Ln bridges resulted in a novel 3D network (Figure.3). The $Se(1)O_3$ group serves as a tetradentate metal linker and bonds to three Eu(1) and one Eu(2) atoms whereas the $Se(2)O_3$ group serves as a hexadentate metal linker bridging with three Eu(III) atoms and three Mo(VI) atoms.

It is interesting to compare the above two structures with those of $Nd_2MoSe_2O_{10}$ and $Gd_2MoSe_3O_{12}$ we previously reported. The lanthanide selenite architectures are different: $[Ln_2(SeO_3)_2(H_2O)]^{2+}$ chains are found in compounds **1** and **3** whereas $Gd_2MoSe_3O_{12}$ features a 2D $[Gd_2(SeO_3)_3]$ layer and a 3D $[Nd_2(SeO_3)_2]^{2+}$ architecture is formed in $Nd_2MoSe_2O_{10}$.[10] Furthermore, one-dimensional (1D) chains of $[Mo_3O_{14}]^{10-}$ clusters composed of edge-sharing of MoO_6 octahedra were observed in compounds **1** and **3** whereas MoO_4 tetrahedra or MoO_6 octahedra in $Nd_2MoSe_2O_{10}$ and $Gd_2MoSe_3O_{12}$ remain "isolated".

Infrared Absorption Spectrum Analyses. The infrared spectra of compounds **1**−**5** display similar features (Supporting Information, Figure S2). They revealed the Se−O and Mo−O vibrations between 400 and 1000 cm^{-1}. The bands between 826 and 986 cm^{-1} and those between 544 and 577 cm^{-1} can be assigned to ν(Mo−O) vibrations, whereas the bands between 610 and 802 cm^{-1} are originated from ν(Se−O) vibrations. The bands from 420 to 530 cm^{-1} may be assigned ν(Se−O−Se). The absorption bands in the range of 3000−3500 and 1400−1650 cm^{-1} can be assigned to water molecular. All of the assignments are in consistent with those previously reported.[1b,10] The observed absorption bands are listed in Supporting Information, Table S2.

Thermal Stability Studies. TGA analyses under a nitrogen atmosphere indicate that these compounds are stable up to 320 °C for **1**, 310 °C for **2**, 285 °C for **3**, 280 °C for **4** and **5**, respectively (Figure 5).

For compounds **1** and **2**, they exhibit two steps of weight losses. The weight losses in the temperature ranges of 320−570 °C and 310−650 °C, correspond to the evaporation of coordinated water and SeO_2 formed by decomposition, which is in agreement with the endothermic peaks at 360 °C, 448 and 554 °C, 320 °C, 450 °C, and 590 °C, respectively, in their DSC diagrams (Supporting Information, Figure S3). Powder X-ray diffraction (PXRD) studies of decomposition products at 650 °C indicated that the residuals are mainly $La_2Mo_4O_{14}$ and $Nd_2Mo_3O_{12}$ combined with some unknown phases (Supporting Information, Figure S4). The observed weight losses of 19.3% and 20.9% for compounds **1** and **2**, respectively, are very close to the calculated ones (20.0% and 19.9%). The second weight losses occurred above 750 °C, indicating further decompositions for each compound, which is consist with the endothermic peaks at 846 and 826 °C (Supporting Information, Figure S3). The decomposition is not complete at 1000 °C. The total weight losses are 22.3% and 23.6% for **1** and **2**, respectively.

Compounds **3**, **4**, and **5** display one main step of weight loss in the temperature ranges of 260−900 °C, 280−660 °C, and 280−595 °C, respectively, in agreement with the endothermic peaks at 360, 482, 530, and 697 °C for **3**, 335, 478, and 517 °C for **4**, 290 and 475 °C for **5** (Supporting Information, Figure S3). The weight losses correspond to the release of 2 mol of SeO_2 and 1 mol of H_2O per formula unit. The observed weight losses are 25.1%, 24.4%, and 24.3%, respectively for **3**, **4**, and **5**, which are slightly larger than the calculated ones (23.5%, 23.0%, and 22.8%). The decomposition products for **3** at 900 °C, **4** and **5** at 680 °C were analyzed by PXRD (Supporting Information, Figure S4). The residual of compound **4** was shown to be $Dy_2Mo_3O_{12}$ whereas those of compounds **3** and **5** are mainly $Eu_2Mo_3O_{12}$ or $Er_2Mo_4O_{15}$ mixed with some unidentified phases.

TG-MS analysis was performed to investigate the decomposition of the water molecules (Figure 5). For the five compounds, a red (m/z = 17) and a blue (m/z = 18) curve with the same shape were observed, indicating that the released gas is water steam (H_2O, m/z = 18; HO^-, m/z = 17) (Supporting Information, Figure S5). From the TG-MS profile, we can see that the release of the ligand occurred in the temperature range of 330−560 °C, 310−530 °C, 290−540 °C, 300−600 °C, and 300−560 °C, with the maximum values at 457, 442, 465, 482, and 480 °C, respectively (Figure 5). It is noticed that the releases of aqua ligand almost exist in the first step of the weight losses for **1** and **2** and the whole process of weight losses for **3**, **4**, and **5**. PXRD studies of the dehydrated products indicate that they exhibit different patterns (heating for 2 h at 450 °C for **1** and **2**; 480 °C for **3**, **4**, and **5**) (Supporting Information, Figure S4). Hence, it can be concluded that the structures collapsed after the removal of H_2O.

dx.doi.org/10.1021/ic200149y |*Inorg. Chem.* 2011, 50, 4934–4943

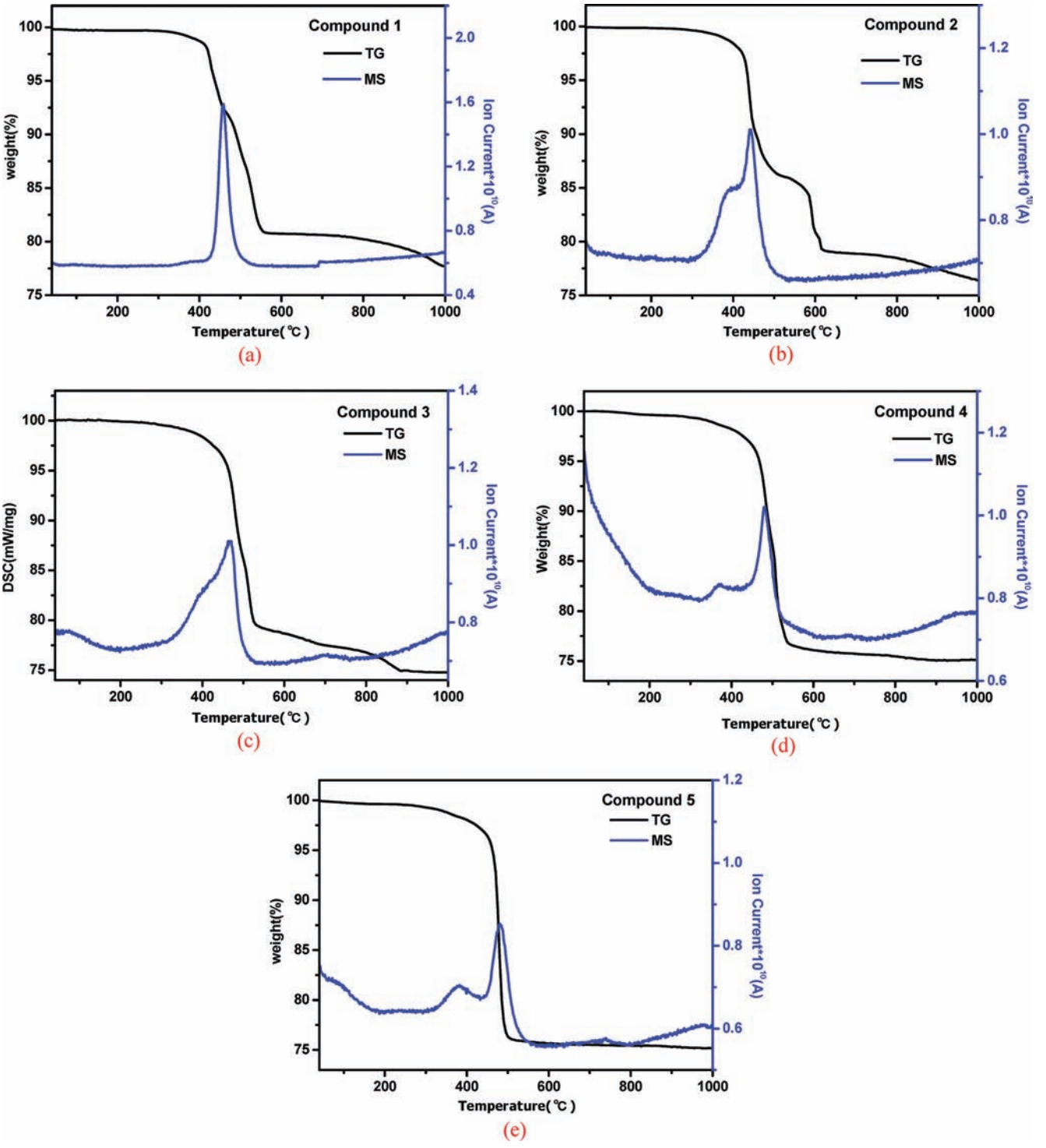

Figure 5. MS-TG curves for compounds **1**−**5**.

Luminescent Properties. The solid state luminescent properties of compounds **2** and **3** were investigated both at room temperature and at 10 K.

Under excitation at 392 nm, compound **2** displays three sets of characteristic emission bands associated with the Nd(III) ion in the near-IR region: $^4F_{3/2} \rightarrow {}^4I_{9/2}$, $^4F_{3/2} \rightarrow {}^4I_{11/2}$, and $^4F_{3/2} \rightarrow {}^4I_{13/2}$ (Supporting Information, Figure S6a).[19] $^4F_{3/2} \rightarrow {}^4I_{9/2}$ is the second largest peak observed and appears as a broad peak covering a 50 nm range. Closer inspection reveals a fine structure of four closely spaced peaks. The dominant peak is $^4F_{3/2} \rightarrow {}^4I_{11/2}$, which is made up of a single intense peak with a secondary shoulder with the intensity about half of the main band. The very weak $^4F_{3/2} \rightarrow {}^4I_{13/2}$ transition band appears at 1331 nm. The weak intensity of the $^4F_{3/2} \rightarrow {}^4I_{13/2}$ band compared with the other two bands can be due to two different gratings used (1200 line/mm grating for the 850−1125 nm range and 300 line/mm grating for the 1300−1450 nm range).

dx.doi.org/10.1021/ic200149y |*Inorg. Chem.* 2011, 50, 4934–4943

Table 2. Observed Emission Bands (nm) for Compounds 2 and 3 at Room Temperature and 10 K

	RT	10 K
	Compound **2**	
$^4F_{3/2} \rightarrow {}^4I_{9/2}$	865.1, 874.5, 891.3, 901.8	874.6, 878.5, 885.2, 891, 898.8, 902.7
$^4F_{3/2} \rightarrow {}^4I_{11/2}$	1042, 1057, 1075	1055.7, 1059.5, 1065.2, 1070.1, 1074, 1076.6, 1083.6
$^4F_{3/2} \rightarrow {}^4I_{13/2}$	1331.3	1330.6, 1335
	Compound **3**	
$^5D_0 \rightarrow {}^7F_0$	580	579.9, 580.5
$^5D_0 \rightarrow {}^7F_1$	588, 594, 599	588.2, 591.8, 592.8, 593.5, 594.3, 598.8
$^5D_0 \rightarrow {}^7F_2$	613, 618, 624	609.6, 613, 613.9, 616.6, 617.9, 620.9, 624.7
$^5D_0 \rightarrow {}^7F_3$	651, 655	650.8, 656.4
$^5D_0 \rightarrow {}^7F_4$	690, 698, 704	691, 693.8, 694.8, 697.7, 701.2, 703.7, 704.3, 706.4

Since compound **2** contains two unique Nd(III) atoms with a low symmetry of C_1, the above transition bands were split into several subbands because of the so-called crystal field effect (for Nd^{3+} ions, the $^{2S+1}L_J$ states will split into $(2J + 1)/2$ sub-bands since L is odd). The $^4F_{3/2}$ is expected to split into 2 sublevels, whereas the complete degeneracy of $^4I_{9/2}$, $^4I_{11/2}$, and $^4I_{13/2}$ leads to 5, 6, and 7 sublevels, respectively. Therefore, $^4F_{3/2} \rightarrow {}^4I_{9/2}$, $^4F_{3/2} \rightarrow {}^4I_{11/2}$, and $^4F_{3/2} \rightarrow {}^4I_{13/2}$ transitions will have a maximum of 10, 12, and 14 sub-bands if both the lower and the upper levels of $^4F_{3/2}$ are populated for a Nd(III) compound with one unique low symmetric Nd(III) site.[20] If a compound contains two and more unique Nd(III) sites located at low symmetry sites, its spectrum will be even more complicated. Because of the overlapping of some emission bands and the resolution limit of the instruments, the observed emission peaks at room temperature are usually much fewer than expected. At a low temperature of 10 K, the lower level is the most populated, whereas the upper level is almost unpopulated; hence, the corresponding emission spectra have much better resolution.[10] Because compound **2** contains two unique Nd sites with C_1 symmetry, it is expected that their emission spectra will display 10, 12, and 14 sub-bands for the $^4F_{3/2} \rightarrow {}^4I_{9/2}$, $^4F_{3/2} \rightarrow {}^4I_{11/2}$, and $^4F_{3/2} \rightarrow {}^4I_{13/2}$ transitions. Upon excitation at 370 nm, compound **2** displays 6 and 7 subbands for the $^4F_{3/2} \rightarrow {}^4I_{9/2}$ and $^4F_{3/2} \rightarrow {}^4I_{11/2}$ transitions at 10 K (Table 2).

The europium emission spectrum obtained for compound **3** principally arises from transitions originating at the $^5D_0$ level. Upon excitation at 395 nm, it exhibits a number of characteristic emission bands associated with the Eu(III) ion: 579 nm ($^5D_0 \rightarrow {}^7F_0$), 587, 593, and 598 nm ($^5D_0 \rightarrow {}^7F_1$), 613, 617, and 623 nm ($^5D_0 \rightarrow {}^7F_2$), very weak band near 650 nm ($^5D_0 \rightarrow {}^7F_3$) transition, and 690, 698, and 709 nm ($^5D_0 \rightarrow {}^7F_4$) (Supporting Information, Figure S7a). It is well-known that the transition $^5D_0 \rightarrow {}^7F_0$ is strictly forbidden in a field of high symmetry. The dominant mechanism of the $^5D_0 \rightarrow {}^7F_0$ line (forbidden by electric-dipole and magnetic-dipole rules) is generally attributed to the borrowing of intensity from the hypersensitive $^5D_0 \rightarrow {}^7F_2$ transition through crystal-field-induced J mixing. The emission band at 579 nm ($^5D_0 \rightarrow {}^7F_0$) indicates that the Eu^{III} ion in **3** should occupy sites with a low symmetry and no inversion center should be present for these sites.[21] It is also noted that the relative intensity of the $^5D_0 \rightarrow {}^7F_2$ and $^5D_0 \rightarrow {}^7F_1$ transition is widely used as a measure of the site symmetry of the europium ion, since the $^5D_0 \rightarrow {}^7F_1$ emission is independent of the ligand environment, and primarily magnetic dipole in character, while the $^5D_0 \rightarrow {}^7F_2$ emission (so-called "hypersensitive" transition) is essentially pure electric dipole in character, and its intensity is very sensitive to the crystal field symmetry. Among the $^5D_0 \rightarrow {}^7F_J$ transitions, only $^5D_0 \rightarrow {}^7F_1$ satisfies the $\Delta J = 0, 1, -1$ (excluding $J = J' = 0$) intermediate coupling selection rule for magnetic dipole intensity, so its intensity is predicted to be primarily magnetic dipole in nature and only weakly dependent on crystal field effects. The remaining transitions can acquire magnetic dipole intensity only via crystal-field-induced J-level mixing.[22] The intensity of the emitting band at 613 nm ($^5D_0 \rightarrow {}^7F_2$) is more intense than the others, indicating that there is no inversion center in the site of the Eu^{3+} ion and it should be responsible for the brilliant-red emission of the complexe.[23]

Since compound **3** contains two independent Eu(III) sites with C_s symmetry, each transition band was expected to split into several sub-bands (for Eu^{3+} ions, the $^{2S+1}L_J$ states will split into $2J + 1$ sub-bands since L is a even) because of the crystal effect field.[24] The complete degeneracy of $^7F_1$, $^7F_2$, $^7F_3$, and $^7F_4$ will split into 3, 5, 7, and 9 subbands whereas the $^5D_0$ and $^7F_0$ will not be populated. So $^5D_0 \rightarrow {}^7F_0$, $^5D_0 \rightarrow {}^7F_1$, $^5D_0 \rightarrow {}^7F_2$, $^5D_0 \rightarrow {}^7F_3$, and $^5D_0 \rightarrow {}^7F_4$ will have a maximum of 1, 3, 5, 7, and 9 sub-bands for a compound containing one unique low symmetric Eu(III) site if the transition bands are populated. At very low temperature such as at 10 K, the corresponding emission spectra have better resolution. The low temperature emission spectra for compound **3** displays 2, 6, 7, and 8 subbands for the $^5D_0 \rightarrow {}^7F_0$, $^5D_0 \rightarrow {}^7F_1$, $^5D_0 \rightarrow {}^7F_2$, and $^5D_0 \rightarrow {}^7F_4$ transitions (Table 2). The observation of two $^5D_0 \rightarrow {}^7F_0$ and six $^5D_0 \rightarrow {}^7F_1$ transition bands indicate there are two unique Eu^{3+} ions, which is also confirmed by the results of structural refinements. The emission peaks observed for $^5D_0 \rightarrow {}^7F_2$, $^5D_0 \rightarrow {}^7F_3$, and $^5D_0 \rightarrow {}^7F_4$ are fewer than expected because of the overlapping of some emission bands and the resolution limit of the instrument. The lifetime of the Eu($^5D_0$) state for $\lambda_{ex,\ em}$ = 465, 613 nm is measured to be about 0.57 ms (Supporting Information, Figure S8).

Phosphorescent emission spectra for compounds **4** and **5** yielded no discernible transitions. This is most probably due to the vibrational mixing of excited states.[25] These metals have a number of internal energy levels between the lowest emissive level (Dy^{3+}: $^4F_{9/2}$; Er^{3+}: $^4I_{13/2}$) and the ground state (Dy^{3+}: $^6H_{15/2}$; Er^{3+}: $^4I_{15/2}$) providing an efficient deactivation pathway of the excited state through vibrational relaxation. Furthermore, the "quenching effect" of the aqua ligands coordinated to the metals may also cause the decrease or even the loss of the ability of luminescence, because the vibrations of the aqua ligands can effectively remove the electronic energy of the excited ions.[26]

Magnetic Properties. Magnetic susceptibility data for compounds **2**−**5** have been studied at a magnetic field of 1000 Oe in the temperature range 2−300 K. Since Mo^{6+} and Se^{4+} are diamagnetic, the paramagnetic contributions are expected to come solely from the Ln^{3+} ions.

The difficulty in studying the magnetic properties of compounds containing paramagnetic Ln^{III} ions originates from the fact that most of the Ln^{III} ions possess a first-order angular momentum. For the $4f^n$ configuration of an Ln^{III} ion, it splits into $^{2S+1}L_J$ states by interelectronic repulsion and spin−orbit coupling. The $^{2S+1}L_J$ states will further split into Stark sublevels

dx.doi.org/10.1021/ic200149y |*Inorg. Chem.* 2011, 50, 4934–4943

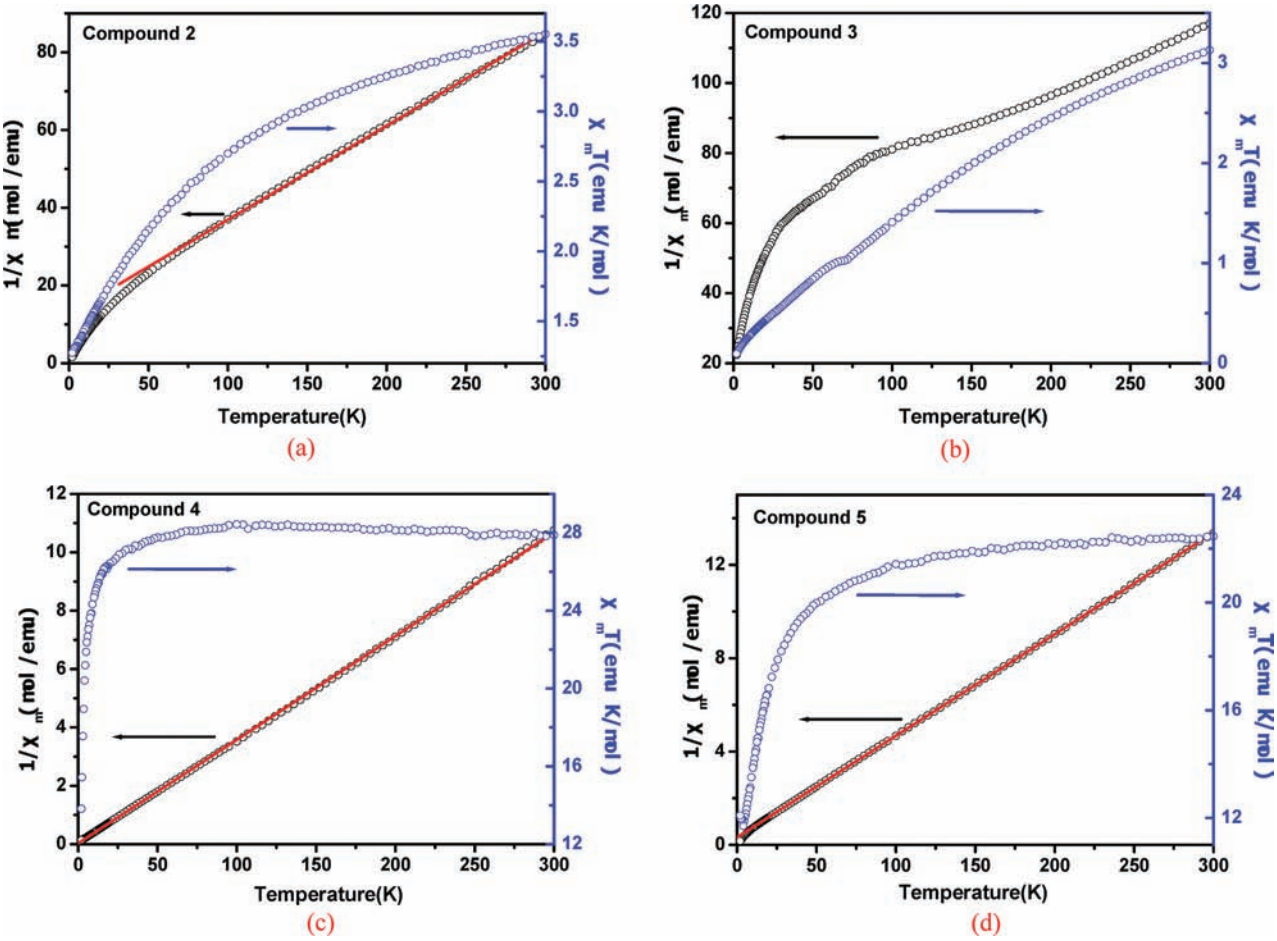

Figure 6. Plots of χ_M^{-1} and $\chi_M T$ versus T for compounds **2**−**5**.

because of crystal-field perturbation. At room temperature, all the Stark levels are populated, but as the temperature decreases, the effective magnetic moment of the lanthanide ion will change by the depopulation of the Stark sublevels, even for a mononuclear Ln^{III} complex. It is the temperature dependence of the Stark sublevels that causes the magnetic susceptibility to deviate from the Curie behavior. This phenomenon is intrinsic to the lanthanide ion and is modulated by the crystal field and the site symmetry of the lanthanide ion.[27]

In the experimental $\chi_M T$ versus T curve for compound **2**, there is a continuous decrease in the value of $\chi_M T$ as the temperature is lowered from room temperature to 2.0 K (Figure 6a). At 300 K, the $\chi_M T$ value is 3.55 emu·mol^{-1}·K, slightly larger than the theoretical one for two isolated Nd(III) ions per formula unit (3.28 emu·mol^{-1}·K), which include the contributions from the spin−orbital interactions. At 2.0 K, it becomes 1.27 emu·mol^{-1}·K. The occurrence of this behavior is attributed to the splitting of the $^4I_{9/2}$ free ion ground state in the crystal field.[28] At room temperature, all the Stark levels arising from the degenerate $^4I_{9/2}$ ground states are populated, but as the temperature decreases, a progressive depopulation of these levels occurs. In the 50−300 K temperature range, the magnetic susceptibility data was described by Curie−Weiss fitting [$\chi_M = C/(T - \theta)$] with C = 4.2 emu·mol^{-1} and θ = −52.6 K. The negative value of θ is due primarily to splitting of the crystal field of the Nd(III) ions as a result of strong spin−orbital coupling and is attributed partly to the possibly antiferromagnetic intrachain coupling. The large θ value indicates the importance of crystal-field effect in compound **2**. It should be mentioned that the nature of the interactions between the Ln^{III} ions with a first-order orbital momentum, such as Nd^{3+} ions, can not simply be deduced from the shape of the $\chi_M T$ versus T curve and the θ value alone.[29]

For compound **3**, the $\chi_M T$ value decreases almost linearly as the temperature is lowered from 300 to 2.0 K, which should be mainly attributed to the depopulation of the Stark levels with nonzero J values for a single Eu^{III} ion (Figure 6b). The observed $\chi_M T$ value at 300 K is 3.13 emu·mol^{-1}·K, slightly larger than the value 3.06 for two isolated Eu(III) ions calculated based on the van Vleck formula allowing for population of the lower-excited state with higher values of J at room temperature. At the lowest temperature, $\chi_M T$ is close to zero (0.092 emu·mol^{-1}·K), indicating a J = 0 ground state of the Eu(III) ion ($^7F_0$).[30] From the curve of χ_M^{-1} versus T, we can see that the magnetic behavior of compound **3** follows the Curie−Weiss law in the temperature range of 300−180 K and then deviated from the law seriously. The presence of thermally populated excited states of Eu^{3+} ions at high temperature and the depopulation of the populated stark sublevels as temperature lowered may account for the behavior. What is more, the $^7F_0$ ground state of Eu^{3+} ion is nonmagnetic (J = 0). Such magnetic behavior has been reported in other Eu^{3+} compounds.[31]

The resulting plots of $\chi_M T$ and $1/\chi_M$ versus T for compound **4** are depicted in Figure 6c. At 300 K, the $\chi_M T$ value is 27.89 emu·mol^{-1}·K, close to the theoretical values of 28.34 emu·mol^{-1}·K

dx.doi.org/10.1021/ic200149y |*Inorg. Chem.* 2011, 50, 4934–4943

for two isolated Dy(III) ions ($S = 5/2$, $L = 5$, $^6H_{15/2}$, and $g = 4/3$) with a $^6H_{15/2}$ ground multiplet well-separated from excited ones. Upon cooling to 30 K, the $\chi_M T$ value remains almost unchanged, and then it decreases sharply and reaches 13.82 emu·mol^{-1}·K at 2.0 K, which probably can be ascribed to a combination of the exchange interaction between the Dy^{III} ions and the splitting of the crystal field of Dy^{III} ions. Curie−Weiss Fitting in the whole experimental region gives the Weiss constant (θ) of −0.80 K and the Curie constant (C) of 2.82 emu·mol^{-1}, which provides further evidence of the progressive depopulation of excited Stark sublevels and weak antiferromagnetic coupling between the Dy^{III} ions. The possible interaction path is Dy−O−Dy bridges and Dy−O−Se−O−Dy bridges with the Dy···Dy separations of 4.011(3) and 7.188(1) Å.

Plots of $\chi_M T$ and $1/\chi_M$ versus T for compounds **5** are shown in Figure 6d. Compound **5** obeys the Curie−Weiss law in the whole experimental region. At 300 K, the $\chi_M T$ value is 22.46 emu·mol^{-1}·K, which is smaller than the theoretical value of 22.96 emu·mol^{-1}·K for two isolated Er(III) ions ($S = 3/2$, $L = 6$, $^4I_{15/2}$, and $g = 6/5$), calculated according to the Van Vleck formula, which includes the contributions from the spin−orbital interactions.[32] On cooling the temperature, the $\chi_M T$ value decreases continuously and reaches a value of 12.10 emu·mol^{-1}·K at 2.0 K, which is primarily due to antiferromagetic interaction between the Er^{III} centers and the splitting of the crystal field of Er^{III} ions. It is expected that the antiferromagnetic interactions occur mainly between magnetic centers within the erbium selenite chains. Linear fitting of $1/\chi_M$ with T according to the Curie−Weiss law gives the Weiss constant (θ) of −7.44 K and the Curie constant (C) of 23.3 emu·mol^{-1}. The magnetic interactions should be dominated by the magnetic exchange interactions between erbium centers through Er−O−Er and Er−O−Se−O−Er bridges with the Er···Er separations of 3.992(6) and 7.172(1) Å. More detailed calculations of these magnetic interactions were not performed because of the complexity of the structures as well as the lack of available suitable models.

CONCLUSIONS

In summary, a series of Mo-rich lanthanide molybdenum selenites with 3D frameworks have been successfully prepared by hydrothermal reactions. It is interesting to note that the MoO_6 octahedra in the structures are polymerized into a molybdenum oxide chain based on trinuclear cluster units whereas the MoO_4 or MoO_6 polyhedra in the lanthanide molybdenum selenites or tellurites reported before remain "isolated". In compounds **3**−**5**, each $[Mo_3O_{14}]^{10-}$ trimer is capped by a Se atom into a $[Mo_3SeO_{14}]^{6-}$ unit and such units are interconnected via corner-sharing into a 1D $[Mo_3SeO_{13}]^{4-}$ anionic chain. In compounds **1** and **2**, two such 1D $[Mo_3SeO_{13}]^{4-}$ anionic chains are interconnected by a 1D $[Mo_{1.75}O_8]^{5.5-}$ chain into a $[Mo_{4.75}SeO_{19}]^{5.5-}$ ribbon. It is anticipated that many other new W-rich or V-rich lanthanide selenites or tellurites can be obtained by similar synthetic methods. Our future research efforts will be devoted to the syntheses, crystal structures, and physical properties of such compounds.

ASSOCIATED CONTENT

Supporting Information. Table of important bond lengths, table of infrared vibration bands, IR spectra, simulated and experimental XRD powder patterns, DSC diagrams, MS curves, PXRD patterns of the decomposed and dehydrated products for **1**−**5**, emission spectra of **2** and **3** at room temperature and 10 K, and luminescent lifetime measurement for **3**. This material is available free of charge via the Internet at http://pubs.acs.org.

AUTHOR INFORMATION

Corresponding Author

*E-mail: mjg@fjirsm.ac.cn.

ACKNOWLEDGMENT

This work was supported by National Natural Science Foundation of China (Nos. 20731006, 20825104, and 20821061).

REFERENCES

(1) (a) Wickleder, M. S. *Chem. Rev.* **2002**, *102*, 2011, and references therein. (b) Verma, V. P. *Thermochim. Acta* **1999**, *327*, 63, and references cited therein. (c) Halasyamani, P. S.; Poeppelmeier, K. R. *Chem. Mater.* **1998**, *10*, 2753.

(2) (a) Kim, S.-H.; Yeon, J.; Halasyamani, P. S. *Chem. Mater.* **2009**, *21*, 5335. (b) Ok, K. -M.; Bhuvanesh, N. S. P.; Halasyamani, P. S. *Inorg. Chem.* **2001**, *40*, 1978. (c) Kong, F.; Huang, S. P.; Sun, Z. M.; Mao, J. G.; Cheng, W. D. *J. Am. Chem. Soc.* **2006**, *128*, 7750. (d) Porter, Y.; Bhuvanesh, N. S. P.; Halasyamani, P. S. *Inorg. Chem.* **2001**, *40*, 1172. (e) Kim, M. K.; Kim, S.-H.; Chang, H.-Y.; Halasyamani, P. S.; Ok, K. M. *Inorg. Chem.* **2010**, *49*, 7028.

(3) (a) Ra, H.-S.; Ok, K.-M.; Halasyamani, P. S. *J. Am. Chem. Soc.* **2003**, *125*, 7764. (b) Ok, K.-M.; Halasyamani, P. S. *Inorg. Chem.* **2004**, *43*, 4248. (c) Chang, H.-Y.; Kim, S. W.; Halasyamani, P. S. *Chem. Mater.* **2010**, *22*, 3241. (d) Chang, H. Y.; Kim, S.-H.; Ok, K.-M.; Halasyamani, P. S. *Chem. Mater.* **2009**, *21*, 1654. (e) Jiang, H. L.; Huang, S. P.; Fan, Y.; Mao, J. G. *Chem.—Eur. J.* **2008**, *14*, 1972. (f) Ok, K. M.; Halasyamani, P. S. *Chem. Soc. Rev.* **2006**, *35*, 710.

(4) (a) Harrison, W. T. A.; Dussack, L. L.; Jacobson, A. J. *Inorg. Chem.* **1994**, *33*, 6043. (b) Johnston, M. G.; Harrison, W. T. A. *Acta Crystallogr., Sect. C* **2007**, *63*, i57. (c) Kwon, Y.-U.; Lee, K.-S.; Kim, Y. H. *Inorg. Chem.* **1996**, *35*, 1161. (d) Balraj, V.; Vidyasagar, K. *Inorg. Chem.* **1999**, *38*, 5809.

(5) (a) Hou, J. Y.; Huang, C. C.; Zhang, H. H.; Tu, C. Y.; Sun, R. Q.; Yang, Q. Y. *J. Mol. Struct.* **2006**, *785*, 37. (b) Harrison, W. T. A.; Dussack, L. L.; Jacobson, A. J. *J. Solid State Chem.* **1996**, *125*, 234. (c) Hou, J. Y.; Huang, C. C.; Zhang, H. H.; Yang, Q. Y.; Chen, Y.-P.; Xu, J.-F. *Acta Crystallogr., Sect. C* **2005**, *61*, i59. (d) Sivakumar, T.; Ok, K. M.; Halasyamani, P. S. *Inorg. Chem.* **2006**, *45*, 3602. (e) Harrison, W. T. A.; Vaughey, J. T.; Goshorn, J. W. *J. Solid State Chem.* **1995**, *116*, 77. (f) Zhang, S. Y.; Hu, C. L.; Sun, C. F.; Mao, J. G. *Inorg. Chem.* **2010**, *49*, 11627.

(6) (a) Zhang, S. Y.; Jiang, H. L.; Sun, C. F.; Mao, J. G. *Inorg. Chem.* **2009**, *48*, 11809. (b) Jiang, H. L.; Xie, Z.; Mao, J. G. *Inorg. Chem.* **2007**, *46*, 6495. (c) Ling, J.; Albrecht-Schmitt, T. E. *J. Solid State Chem.* **2007**, *180*, 1601. (d) Zhou, Y.; Hu, C. L.; Hu, T.; Kong, F.; Mao, J. G. *Dalton Trans.* **2009**, 5747. (e) Pitzschke, D.; Jansen, M. *Z. Anorg. Allg. Chem.* **2007**, *633*, 1563. (f) Jiang, H. L.; Kong, F.; Fan, Y.; Mao, J. G. *Inorg. Chem.* **2008**, *47*, 7430.

(7) (a) Kong, F.; Hu, C. L.; Hu, T.; Zhou, Y.; Mao, J. G. *Dalton Trans.* **2009**, 4962. (b) Ok, K. M.; Halasyamani, P. S. *Chem. Mater.* **2002**, *14*, 2360. (c) Ok, K. M.; Halasyamani, P. S. *Chem. Mater.* **2001**, *13*, 4278. (d) Li, P. X.; Kong, F.; Hu, C. L.; Zhao, N.; Mao, J. G. *Inorg. Chem.* **2010**, *49*, 5943. (e) Kong, F.; Xu, X.; Mao, J. G. *Inorg. Chem.* **2010**, *49*, 11573.

(8) (a) Wontcheu, J.; Schleid, T. *J. Solid State Chem.* **2003**, *171*, 429. (b) Wontcheu, J.; Schleid, T. *Z. Anorg. Allg. Chem.* **2002**, *628*, 1941. (c) Ruck, M.; Schmidt, P. *Z. Anorg. Allg. Chem.* **2003**, *629*, 2133. (d) Wontcheu, J.; Schleid, T. *Z. Anorg. Allg. Chem.* **2003**, *629*, 1463.

(e) Krugermann, I.; Wickleder, M. S. *J. Solid State Chem.* **2002**, *167*, 113. (f) Krugermann, I.; Wickleder, M. S. *Z. Anorg. Allg. Chem.* **2002**, *628*, 147.

(9) (a) Ljjaali, I.; Flaschenrien, C.; Ibers, J. A. *J. Alloys Compd.* **2003**, *354*, 115. (b) Weber, F. A.; Meier, S. F.; Schleid, T. *Z. Anorg. Allg. Chem.* **2001**, *627*, 2225. (c) Meier, S. F.; Weber, F. A.; Glaser, R. J.; Schleid, T. *Z. Anorg. Allg. Chem.* **2001**, *627*, 2448. (d) Shen, Y. L.; Mao, J.-G. *J. Alloys Compd.* **2004**, *385*, 86.

(10) (a) Shen, Y.-L.; Jiang, H.-L.; Xu, J.; Mao, J.-G.; Cheah, K. W. *Inorg. Chem.* **2005**, *44*, 9314. (b) Jiang, H.-L.; Ma, E.; Mao, J.-G. *Inorg. Chem.* **2007**, *46*, 7012.

(11) Li, P.-X.; Zhang, S.-Y.; Mao, J.-G. *Dalton Trans.* **2010**, *39*, 11560.

(12) Wendlandt, W. M.; Hecht, H. G. *Reflectance Spectroscopy*; Interscience: New York, 1966.

(13) (a) *CrystalClear*, Version 1.3.5; Rigaku Corp.: Woodlands, TX, 1999. (b) Sheldrick, G. M. *SHELXTL*, Crystallographic Software Package, Version 5.1; Bruker-AXS: Madison, WI, 1998. (c) Spek, A. L. *J. Appl. Crystallogr.* **2003**, *36*, 7.

(14) (a) Zhang, X. T.; Wang, D. Q.; Dou, J. M.; Yan, S. S.; Yao, X. X.; Jiang, J. Z. *Inorg. Chem.* **2006**, *45*, 10629. (b) Long, D.-L.; Kögerler, P.; Parenty, A. D. C.; Fielden, J.; Cronin, L. *Angew. Chem., Int. Ed.* **2006**, *45*, 4798.

(15) (a) Wickleder, M. S. *Z. Anorg. Allg. Chem.* **2000**, *626*, 547.

(16) (a) Halasyamani, P.-S. *Chem. Mater.* **2004**, *16*, 3586. (b) Porter, Y.; Halasyamani, P. S. *J. Solid State Chem.* **2003**, *174*, 441.

(17) (a) Balraj, V.; Vidyasagar, K. *Inorg. Chem.* **1998**, *37*, 4764. (b) Balraj, V.; Vidyasagar, K. *Inorg. Chem.* **1999**, *38*, 1394.

(18) (a) Guesdon, A.; Raveau, B. *Chem. Mater.* **2000**, *12*, 2239. (b) Chi, E. O.; Ok, K. M.; Porter, Y.; Halasyamani, P. S. *Chem. Mater.* **2006**, *18*, 2070.

(19) (a) Wong, W.-K.; Liang, H.-Z.; Guo, J.-P.; Wong, W.-Y.; Lo, W.-K.; Li, K.-F.; Cheah, K.-W.; Zhou, Z.-Y.; Wong, W.-T. *Eur. J. Inorg. Chem.* **2004**, 829. (b) Song, J.-L.; Lei, C.; Mao, J.-G. *Inorg. Chem.* **2004**, *43*, 5630. (c) Hebbink, G. A.; Grave, L.; Woldering, L. A.; Reinhoudt, D. N.; van Vegel, F. C. J. M. *J. Phys. Chem.* **2003**, *A107*, 2483.

(20) Morrison, C. A.; Leavitt, R. P. . In *Handbook on the Physics and Chemistry of Rare Earth*; Gschneider, K. A., Eyring, L., Eds.; North-Holland Publishing Company: NewYork, 1982; Vol. 5, pp 461−693, and references therein.

(21) (a) Kim, Y. J.; Suh, M.; Jung, D. Y. *Inorg. Chem.* **2004**, *43*, 245. (b) Serre, C.; Pelle, F.; Gardant, N.; Férey, G. *Chem. Mater.* **2004**, *16*, 1177.

(22) (a) Kirby, A. F.; Foster, D.; Richardson, F. S. *Chem. Phys. Lett.* **1983**, *95*, 507. (b) Xu, Q. H.; Li, L. S.; Liu, X. S.; Xu, R. R. *Chem. Mater.* **2002**, *14*, 549.

(23) Qian, G.-D.; Wang, M.-Q. *Mater. Res. Bull.* **2001**, *36*, 2289.

(24) Chen, P. L.; Chiang, P. Y.; Yeh, H. C.; Chang, B. C.; Lii, K. H. *Dalton Trans.* **2008**, 1721.

(25) (a) Sastri, V. S.; Bunzli, J.-C.; Rao, V. R.; Rayudu, G. V. S.; Perumareddi, J. R. *Modern Aspects of Rare Earths and their Complexes*; Elsevier: New York, 2003. (b) Monguzzi, A.; Milani, A.; Lodi, L.; Italo-Trioni, M.; Tubino, R.; Castiglioni, C. *New J. Chem.* **2009**, *33*, 1542.

(26) (a) Auzel, F. *Acad. Sci. Paris* **1966**, 1016.(b) Wright, J. C. *Topics in Applied Physics: Radiationless Processes in Molecules and Condensed Phases*; Fong, F. K., Ed.; Springer: Berlin, 1976; pp 239−295. (c) Layne, B.; Lowdermilk, W. H.; Weber, M. J. *Phys. Rev. B* **1997**, *16*, 10.

(27) (a) Kahn, M. L.; Ballou, R.; Porcher, P.; Kahn, O.; Sutter, J.-P. *Chem.—Eur. J.* **2002**, *8*, 525. (b) Costes, J.-P.; Nicodème, F. *Chem.—Eur. J.* **2002**, *8*, 3442.

(28) Andruh, M.; Bakalbasis, E.; Kahn, O.; Trombe, J. C.; Porcher, P. *Inorg. Chem.* **1993**, *32*, 1616.

(29) Kahn, M. L.; Sutter, J.-P.; Golhen, S.; Guionneau, P.; Ouahab, L.; Kahn, O.; Chasseau, D. *J. Am. Chem. Soc.* **2000**, *122*, 3413.

(30) (a) Lenaerts, P.; Driesen, K.; Deun, R. V.; Binnemans, K. *Chem. Mater.* **2005**, *17*, 2148. (b) He, Z.; Gao, E. Q.; Wang, Z. M.; Yan, C. H.; Kurmoo, M. *Inorg. Chem.* **2005**, *44*, 862. (c) Wang, Y.; Zheng, X.; Zhuang, W.; Jin, L. *Eur. J. Inorg. Chem.* **2003**, 3572.

(31) (a) Yang, J.; Yue, Q.; Li, G.-D.; Cao, J.-J.; Li, G.-H.; Chen, J.-S. *Inorg. Chem.* **2006**, *45*, 2857. (b) Zheng, X. J.; Sun, C. Y.; Lu, S. Z.; Liao, F. H.; Gao, S.; Jin, L. P. *Eur. J. Inorg. Chem.* **2004**, 3262. (c) Zhang, Z.-H.; Okamura, T.; Hasegawa, Y.; Kawaguchi, H.; Kong, L.-Y.; Sun, W.-Y.; Ueyama, N. *Inorg. Chem.* **2005**, *44*, 6219. (d) Wan, Y. H.; Zhang, L. P.; Jin, L. P.; Gao, S.; Lu, S. Z. *Inorg. Chem.* **2003**, *42*, 4985. (e) Du, Z.-Y.; Xu, H.-B.; Mao, J.-G. *Inorg. Chem.* **2006**, *45*, 9780.

(32) Van Vleck, J. H. *The Theory of Electric and Magnetic Susceptibilities*; Oxford University: Oxford, U.K., 1932; pp 226−261.